Supplementary Material to

Urban scale vehicle-to-building-to-grid integration leveraging human mobility modeling for enhanced grid flexibility

Supporting information to https://doi.org/10.1007/s12273-025-1346-3

A. Development of Multi-Zone RC model

With the 28R17C model, building thermal dynamics are written with the temperature states of both walls and zones as equations showing below,

$$\dot{T}_{1w} = \frac{T_0 - T_{1w}}{C_{1w}R_{1w1}} + \frac{T_1 - T_{1w}}{C_{1w}R_{1w2}} + \frac{\dot{Q}_{sol1}}{C_{1w}} \tag{A.1}$$

$$\dot{T}_{14} = \frac{T_4 - T_{14}}{C_{14}R_{142}} + \frac{T_1 - T_{14}}{C_{14}R_{141}} \tag{A.2}$$

$$\dot{T}_{12} = \frac{T_1 - T_{12}}{C_{12}R_{121}} + \frac{T_2 - T_{12}}{C_{12}R_{122}} \tag{A.3}$$

$$\dot{T}_{15} = \frac{T_1 - T_{15}}{C_{15}R_{151}} + \frac{T_5 - T_{15}}{C_{15}R_{152}} \tag{A.4}$$

$$\begin{aligned}\dot{T}_1 = {} & \frac{T_{1w} - T_1}{C_1R_{1w2}} + \frac{T_{15} - T_1}{C_1R_{151}} + \frac{T_0 - T_1}{C_1R_{1win}} + \frac{T_{12} - T_1}{C_1R_{121}} \\ & + \frac{T_{14} - T_1}{C_1R_{141}} + \frac{\dot{Q}_{HVAC1}}{C_1} + \frac{\dot{Q}_{int1}}{C_1}\end{aligned} \tag{A.5}$$

$$\dot{T}_{2w} = \frac{T_0 - T_{2w}}{C_{2w}R_{2w1}} + \frac{T_2 - T_{2w}}{C_{2w}R_{2w2}} + \frac{\dot{Q}_{sol2}}{C_{2w}} \tag{A.6}$$

$$\dot{T}_{23} = \frac{T_2 - T_{23}}{C_{23}R_{231}} + \frac{T_3 - T_{23}}{C_{23}R_{232}} \tag{A.7}$$

$$\dot{T}_{25} = \frac{T_2 - T_{25}}{C_{25}R_{251}} + \frac{T_5 - T_{25}}{C_{25}R_{252}} \tag{A.8}$$

$$\begin{aligned}\dot{T}_2 = &\frac{T_{12} - T_2}{C_2R_{122}} + \frac{T_{23} - T_2}{C_2R_{231}} + \frac{T_{25} - T_2}{C_2R_{251}} + \frac{T_{2w} - T_2}{C_2R_{2w2}} \\ &+ \frac{T_0 - T_2}{C_2R_{2win}} + \frac{\dot{Q}_{HVAC2}}{C_2} + \frac{\dot{Q}_{int2}}{C_2}\end{aligned} \tag{A.9}$$

$$\dot{T}_{3w} = \frac{T_0 - T_{3w}}{C_{3w}R_{3w1}} + \frac{T_3 - T_{3w}}{C_{3w}R_{3w2}} + \frac{\dot{Q}_{sol3}}{C_{3w}} \tag{A.10}$$

$$\dot{T}_{34} = \frac{T_3 - T_{34}}{C_{34}R_{341}} + \frac{T_4 - T_{34}}{C_{34}R_{342}} \tag{A.11}$$

$$\dot{T}_{35} = \frac{T_3 - T_{35}}{C_{35}R_{351}} + \frac{T_5 - T_{35}}{C_{35}R_{352}} \tag{A.12}$$

$$\begin{aligned}\dot{T}_3 = &\frac{T_{23} - T_3}{C_3R_{232}} + \frac{T_{34} - T_3}{C_3R_{341}} + \frac{T_{35} - T_3}{C_3R_{351}} + \frac{T_{3w} - T_3}{C_3R_{3w2}} \\ &+ \frac{T_0 - T_3}{C_3R_{3win}} + \frac{\dot{Q}_{HVAC3}}{C_3} + \frac{\dot{Q}_{int3}}{C_3}\end{aligned} \tag{A.13}$$

$$\dot{T}_{4w} = \frac{T_0 - T_{4w}}{C_{4w}R_{4w1}} + \frac{T_4 - T_{4w}}{C_{4w}R_{4w2}} + \frac{\dot{Q}_{sol4}}{C_{4w}} \tag{A.14}$$

$$\dot{T}_{45} = \frac{T_4 - T_{45}}{C_{45}R_{451}} + \frac{T_5 - T_{45}}{C_{45}R_{452}} \qquad A.15$$

$$\dot{T}_4 = \frac{T_{4w} - T_4}{C_4 R_{4w2}} + \frac{T_{14} - T_4}{C_4 R_{142}} + \frac{T_{34} - T_4}{C_4 R_{342}} + \frac{T_{45} - T_4}{C_4 R_{451}} + \frac{T_0 - T_4}{C_4 R_{4win}} + \frac{\dot{Q}_{HVAC4}}{C_4} + \frac{\dot{Q}_{int4}}{C_4} \qquad A.16$$

$$\dot{T}_5 = \frac{T_{15} - T_5}{C_5 R_{152}} + \frac{T_{25} - T_5}{C_5 R_{252}} + \frac{T_{35} - T_5}{C_5 R_{352}} + \frac{T_{45} - T_5}{C_5 R_{452}} + \frac{\dot{Q}_{HVAC5}}{C_5} + \frac{\dot{Q}_{int5}}{C_5} \qquad A.17$$

$$\begin{aligned}
\dot{Q}_{HVAC1} &= \mu_{HVAC2} \times P_{HVAC1} \\
\dot{Q}_{HVAC2} &= \mu_{HVAC2} \times P_{HVAC2} \\
\dot{Q}_{HVAC3} &= \mu_{HVAC2} \times P_{HVAC3} \\
\dot{Q}_{HVAC4} &= \mu_{HVAC2} \times P_{HVAC4} \\
\dot{Q}_{HVAC5} &= \mu_{HVAC2} \times P_{HVAC5}
\end{aligned} \qquad A.18$$

where, R_{1win} to R_{4win} represent the thermal resistance of windows on exterior walls associated to each zone; And R_{1w} to R_{4w} and R_{121} to R_{452} represent the physical parameters of both the exterior walls and internal walls; C_{1w} to C_{5w} are the lumped thermal capacity of external walls, and C_{12} to C_{45} are the lumped thermal capacity of all internal walls and the roof; $C_1 to$ C_5 are the thermal capacity of the zones; $\dot{Q}_{sol1}$ to $\dot{Q}_{sol4}$ represent the total solar radiation absorbed by the external walls; $\dot{Q}_{int1}$ to $\dot{Q}_{int4}$ are the total internal heat gains from space heat within each zone. T_1 to T_5, and T_{1w} to T_{4w} are the temperature of the zones and external walls respectively; T_{12} to T_{45} represent the temperature for internal walls between adjacent zones; T_0 represents the outside ambient temperature. $\dot{Q}_{hvac1}$ to $\dot{Q}_{hvac5}$ are the

HVAC loads injected into all zones, P_{HVAC1} to P_{HVAC5} represent the power consumed by the HVAC system in each zone, and μ_{HVAC2} is the coefficient of performance of the HVAC system.

Following above equations, the building dynamics can be represented by the state space equation,

$$\dot{x}_n^t = A_n x_n^t + B_n u_n^t + E_n w_n^t \qquad \text{A.19}$$

where x_n^t defined by Equation A.20, is the temperature state of the building n includes exterior and internal walls, as well as the internal zones at time t. u_n^t defined by Equation A.22 is the control input which represents the power consumption of building HVAC systems in each zone. w_n^t defined by Equation A.21 denotes the disturbances of building n caused by outdoor ambient temperature, solar radiation and internal heat gains at time t.

$$x_n^t = [T_{1w}^t \ \ T_{14}^t \ \ T_{12}^t \ \ T_{15}^t \ \ T_1^t \ \ T_{2w}^t \ \ T_{23}^t \ \ T_{25}^t \ \ T_2^t \ \ T_{3w}^t \ \ T_{34}^t \ \ T_{35}^t \ \ T_3^t \ \ T_{4w}^t \ \ T_{45}^t \ \ T_4^t \ \ T_5^t]^T \qquad A.20$$

$$u_n^t = \begin{bmatrix} Q_{HVAC1} \\ Q_{HVAC2} \\ Q_{HVAC3} \\ Q_{HVAC4} \\ Q_{HVAC5} \end{bmatrix} \qquad A.21$$

$$w_n^t = \begin{bmatrix} Q_{sol1} \\ Q_{int1} \\ Q_{sol2} \\ Q_{int2} \\ Q_{sol3} \\ Q_{int3} \\ Q_{sol4} \\ Q_{int4} \\ Q_{int5} \\ T_0 \end{bmatrix} \qquad A.22$$

The system matrices A_n, B_n, E_n are defined as Equation A.23 to Equation A.25 shown below. Compared with 3R2C model, this multi-zone RC model has more complex state space matrices. The discretization approach of this multi-zone RC model follows the same approach in Fontenot et al. (2021).

A_n Matrix.

$$A_n = \begin{bmatrix}
\frac{-1}{C_{1w}\left(\frac{1}{R_{1w1}}+\frac{1}{R_{1w2}}\right)} & \cdot & \cdot & \cdot & \frac{1}{C_{1w}R_{1w2}} & \cdot & \cdot & \cdot & \cdot & \cdot & \cdot & \cdot & \cdot & \cdot & \cdot & \cdot & \cdot \\
\cdot & \frac{-1}{C_{14}\left(\frac{1}{R_{142}}+\frac{1}{R_{141}}\right)} & \cdot & \cdot & \frac{1}{C_{14}R_{141}} & \cdot & \cdot & \cdot & \cdot & \cdot & \cdot & \cdot & \cdot & \cdot & \cdot & \frac{1}{C_{14}R_{142}} & \cdot \\
\cdot & \cdot & \frac{-1}{C_{12}\left(\frac{1}{R_{121}}+\frac{1}{R_{122}}\right)} & \cdot & \frac{1}{C_{12}R_{121}} & \cdot & \cdot & \cdot & \frac{1}{C_{12}R_{122}} & \cdot & \cdot & \cdot & \cdot & \cdot & \cdot & \cdot & \cdot \\
\cdot & \cdot & \cdot & \frac{-1}{C_{15}\left(\frac{1}{R_{151}}+\frac{1}{R_{152}}\right)} & \frac{1}{C_{15}R_{151}} & \cdot & \cdot & \cdot & \cdot & \cdot & \cdot & \cdot & \cdot & \cdot & \cdot & \cdot & \frac{1}{C_{15}R_{152}} \\
\frac{1}{C_1R_{1w2}} & \frac{1}{C_1R_{141}} & \frac{1}{C_1R_{121}} & \frac{1}{C_1R_{151}} & \frac{-1}{C_1\left(\frac{1}{R_{1w2}}+\frac{1}{R_{141}}+\frac{1}{R_{121}}+\frac{1}{R_{151}}+\frac{1}{R_{1win}}\right)} & \cdot & \cdot & \cdot & \cdot & \cdot & \cdot & \cdot & \cdot & \cdot & \cdot & \cdot & \cdot \\
\cdot & \cdot & \cdot & \cdot & \cdot & \frac{-1}{C_{2w}\left(\frac{1}{R_{2w1}}+\frac{1}{R_{2w2}}\right)} & \cdot & \cdot & \frac{1}{C_{2w}R_{2w2}} & \cdot & \cdot & \cdot & \cdot & \cdot & \cdot & \cdot & \cdot \\
\cdot & \cdot & \cdot & \cdot & \cdot & \cdot & \frac{-1}{C_{23}\left(\frac{1}{R_{231}}+\frac{1}{R_{232}}\right)} & \cdot & \frac{1}{C_{23}R_{231}} & \cdot & \cdot & \cdot & \frac{1}{C_{23}R_{232}} & \cdot & \cdot & \cdot & \cdot \\
\cdot & \cdot & \cdot & \cdot & \cdot & \cdot & \cdot & \frac{-1}{C_{25}\left(\frac{1}{R_{251}}+\frac{1}{R_{252}}\right)} & \frac{1}{C_{25}R_{251}} & \cdot & \cdot & \cdot & \cdot & \cdot & \cdot & \cdot & \frac{1}{C_{25}R_{252}} \\
\cdot & \cdot & \frac{1}{C_2R_{122}} & \cdot & \cdot & \frac{1}{C_2R_{2w2}} & \frac{1}{C_2R_{231}} & \frac{1}{C_2R_{251}} & \frac{-1}{C_2\left(\frac{1}{R_{122}}+\frac{1}{R_{2w2}}+\frac{1}{R_{231}}+\frac{1}{R_{251}}+\frac{1}{R_{2win}}\right)} & \cdot & \cdot & \cdot & \cdot & \cdot & \cdot & \cdot & \cdot \\
\cdot & \cdot & \cdot & \cdot & \cdot & \cdot & \cdot & \cdot & \cdot & \frac{-1}{C_{3w}\left(\frac{1}{R_{3w1}}+\frac{1}{R_{3w2}}\right)} & \cdot & \cdot & \frac{1}{C_{3w}R_{3w2}} & \cdot & \cdot & \cdot & \cdot \\
\cdot & \cdot & \cdot & \cdot & \cdot & \cdot & \cdot & \cdot & \cdot & \cdot & \frac{-1}{C_{34}\left(\frac{1}{R_{341}}+\frac{1}{R_{342}}\right)} & \cdot & \frac{1}{C_{34}R_{341}} & \cdot & \cdot & \frac{1}{C_{34}R_{342}} & \cdot \\
\cdot & \cdot & \cdot & \cdot & \cdot & \cdot & \cdot & \cdot & \cdot & \cdot & \cdot & \frac{-1}{C_{35}\left(\frac{1}{R_{351}}+\frac{1}{R_{352}}\right)} & \frac{1}{C_{35}R_{351}} & \cdot & \cdot & \cdot & \frac{1}{C_{35}R_{352}} \\
\cdot & \cdot & \cdot & \cdot & \cdot & \cdot & \frac{1}{C_3R_{232}} & \cdot & \cdot & \frac{1}{C_3R_{3w2}} & \frac{1}{C_3R_{341}} & \frac{1}{C_3R_{351}} & \frac{-1}{C_3\left(\frac{1}{R_{232}}+\frac{1}{R_{3w2}}+\frac{1}{R_{341}}+\frac{1}{R_{351}}+\frac{1}{R_{3win}}\right)} & \cdot & \cdot & \cdot & \cdot \\
\cdot & \cdot & \cdot & \cdot & \cdot & \cdot & \cdot & \cdot & \cdot & \cdot & \cdot & \cdot & \cdot & \frac{-1}{C_{4w}\left(\frac{1}{R_{4w1}}+\frac{1}{R_{4w2}}\right)} & \cdot & \frac{1}{C_{4w}R_{4w2}} & \cdot \\
\cdot & \cdot & \cdot & \cdot & \cdot & \cdot & \cdot & \cdot & \cdot & \cdot & \cdot & \cdot & \cdot & \cdot & \frac{-1}{C_{45}\left(\frac{1}{R_{451}}+\frac{1}{R_{452}}\right)} & \frac{1}{C_{45}R_{451}} & \frac{1}{C_{45}R_{452}} \\
\cdot & \frac{1}{C_4R_{142}} & \cdot & \cdot & \cdot & \cdot & \cdot & \cdot & \cdot & \cdot & \frac{1}{C_4R_{342}} & \cdot & \cdot & \frac{1}{C_4R_{4w2}} & \frac{1}{C_4R_{451}} & \frac{-1}{C_4\left(\frac{1}{R_{142}}+\frac{1}{R_{342}}+\frac{1}{R_{4w2}}+\frac{1}{R_{451}}+\frac{1}{R_{4win}}\right)} & \cdot \\
\cdot & \cdot & \cdot & \frac{1}{C_5R_{152}} & \cdot & \cdot & \cdot & \frac{1}{C_5R_{252}} & \cdot & \cdot & \cdot & \frac{1}{C_5R_{352}} & \cdot & \cdot & \frac{1}{C_5R_{452}} & \cdot & \frac{-1}{C_5\left(\frac{1}{R_{152}}+\frac{1}{R_{252}}+\frac{1}{R_{352}}+\frac{1}{R_{452}}\right)}
\end{bmatrix} \quad \text{A.23}$$

$$B_n = \begin{bmatrix} \cdot & \cdot & \cdot & \cdot & \cdot \\ \cdot & \cdot & \cdot & \cdot & \cdot \\ \cdot & \cdot & \cdot & \cdot & \cdot \\ \cdot & \cdot & \cdot & \cdot & \cdot \\ \frac{1}{C_1} & \cdot & \cdot & \cdot & \cdot \\ \cdot & \cdot & \cdot & \cdot & \cdot \\ \cdot & \cdot & \cdot & \cdot & \cdot \\ \cdot & \cdot & \cdot & \cdot & \cdot \\ \cdot & \frac{1}{C_2} & \cdot & \cdot & \cdot \\ \cdot & \cdot & \cdot & \cdot & \cdot \\ \cdot & \cdot & \cdot & \cdot & \cdot \\ \cdot & \cdot & \cdot & \cdot & \cdot \\ \cdot & \cdot & \frac{1}{C_3} & \cdot & \cdot \\ \cdot & \cdot & \cdot & \cdot & \cdot \\ \cdot & \cdot & \cdot & \cdot & \cdot \\ \cdot & \cdot & \cdot & \frac{1}{C_4} & \cdot \\ \cdot & \cdot & \cdot & \cdot & \frac{1}{C_5} \end{bmatrix} \qquad A.25$$

$$E_n = \begin{bmatrix} \frac{1}{C_{1w}} & \cdot & \cdot & \cdot & \cdot & \cdot & \cdot & \cdot & \cdot & \frac{1}{C_{1w}R_{1w1}} \\ \cdot & \cdot & \cdot & \cdot & \cdot & \cdot & \cdot & \cdot & \cdot & \cdot \\ \cdot & \cdot & \cdot & \cdot & \cdot & \cdot & \cdot & \cdot & \cdot & \cdot \\ \cdot & \cdot & \cdot & \cdot & \cdot & \cdot & \cdot & \cdot & \cdot & \cdot \\ \cdot & \frac{1}{C_1} & \cdot & \cdot & \cdot & \cdot & \cdot & \cdot & \cdot & \frac{1}{C_1R_{win}} \\ \cdot & \cdot & \frac{1}{C_{2w}} & \cdot & \cdot & \cdot & \cdot & \cdot & \cdot & \frac{1}{C_{2w}R_{2w1}} \\ \cdot & \cdot & \cdot & \cdot & \cdot & \cdot & \cdot & \cdot & \cdot & \cdot \\ \cdot & \cdot & \cdot & \cdot & \cdot & \cdot & \cdot & \cdot & \cdot & \cdot \\ \cdot & \cdot & \cdot & \frac{1}{C_2} & \cdot & \cdot & \cdot & \cdot & \cdot & \frac{1}{C_2R_{2win}} \\ \cdot & \cdot & \cdot & \cdot & \frac{1}{C_{3w}} & \cdot & \cdot & \cdot & \cdot & \frac{1}{C_{3w}R_{3w1}} \\ \cdot & \cdot & \cdot & \cdot & \cdot & \cdot & \cdot & \cdot & \cdot & \cdot \\ \cdot & \cdot & \cdot & \cdot & \cdot & \cdot & \cdot & \cdot & \cdot & \cdot \\ \cdot & \cdot & \cdot & \cdot & \cdot & \frac{1}{C_3} & \cdot & \cdot & \cdot & \frac{1}{C_3R_{3win}} \\ \cdot & \cdot & \cdot & \cdot & \cdot & \cdot & \frac{1}{C_{4w}} & \cdot & \cdot & \frac{1}{C_{4w}R_{4w1}} \\ \cdot & \cdot & \cdot & \cdot & \cdot & \cdot & \cdot & \cdot & \cdot & \cdot \\ \cdot & \cdot & \cdot & \cdot & \cdot & \cdot & \cdot & \frac{1}{C_4} & \cdot & \frac{1}{C_4R_{4win}} \\ \cdot & \cdot & \cdot & \cdot & \cdot & \cdot & \cdot & \cdot & \frac{1}{C_5} & \cdot \end{bmatrix} \qquad A.24$$

B. Human Mobility Results for the Target Community

From the GPS dataset, we identified a total of 46,185,937 entries from an average of 439,729 daily users across Arizona. For detailed analysis, a specific census tract within the Phoenix Metropolitan Area was selected. Following methods established in previous studies (Liu 2024; Liu and Dong 2024), we identified anonymized users within this tract and preprocessed the data to extract hourly mobility patterns over a 24-hour period.

Kernel Density Estimators (KDEs) were adopted to statistically model the mobility behavior, including departure and arrival times for home and workplace for each user in the selected tract. Each user's geolocation, estimated from the GPS dataset, was utilized to calculate daily travel distances. Based on the mobility patterns identified, Figure 1 illustrates the probability density distributions of departure and arrival times for home and workplace locations. The data indicate that peak departure times from home occur between 7 AM and 10 AM, while peak arrival times at home range from 3 PM to 8 PM. For workplaces, arrivals peak around 9 AM, and departures peak around 6 PM. These findings are consistent with typical daily schedules of building occupants (Wu et al. 2020).

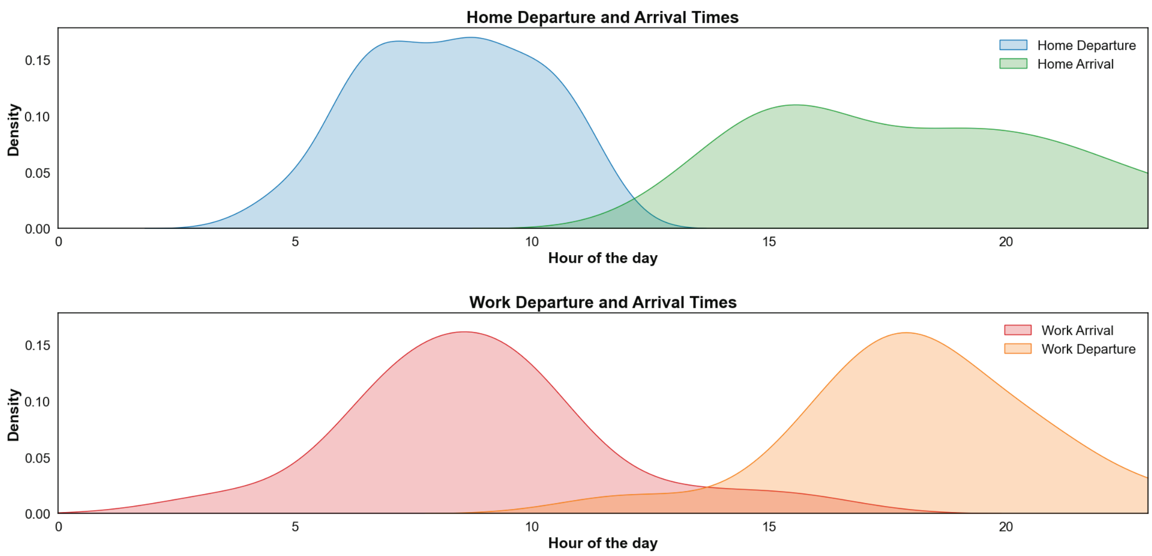

Figure 1. Departure and arrival times for both home and workplace in the target community

In the proposed control framework, users' daily travel patterns were sampled from the KDEs and integrated to infer building occupancy information. For the multi-zone commercial building energy model, zone-level occupancy profiles were generated by combining users' travel patterns (first arrival and last departure) with the Lawrence Berkeley National Laboratory's Occupancy Simulator (Chen et al. 2018). Details on this integration are provided in the following section.

Finally, Figure 2 presents a box plot of total daily travel distances among users in the target community. The maximum daily travel distance on weekdays is approximately 30 km (19 miles). When compared to the estimated driving range of a typical Tesla Model (341 miles, as reported by the U.S. Environmental Protection Agency), this highlights the potential of EV batteries to support building energy needs and enhance grid flexibility.

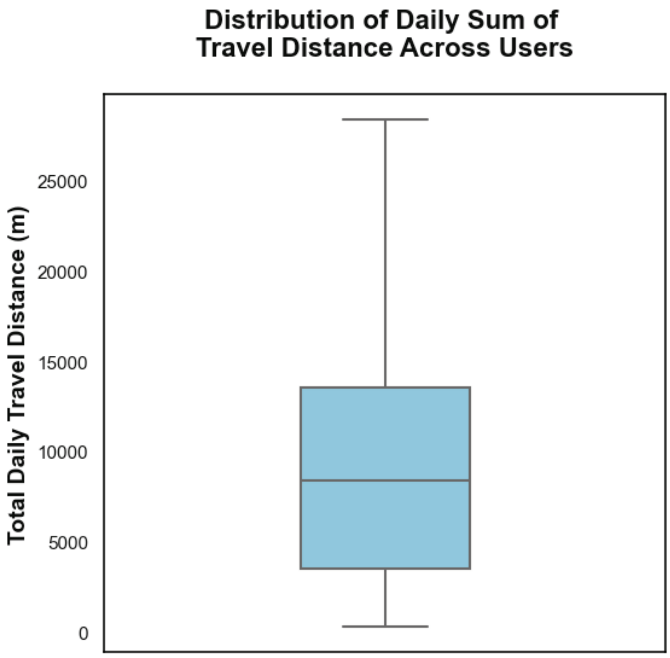

Figure 2. Box plot of total daily travel distance across users in the target community

C. Building RC Model Calibration

Building stocks and geolocations in GIS. In the initial step of preparing input data for EnergyPlus simulations, information on building stocks and geolocations was compiled. We have utilized the building footprints within the Phoenix Metropolitan Area, sourced from the Microsoft Global Building Footprints Database (Microsoft/GlobalMLBuildingFootprints 2024). Through a spatial join operation, the building footprints were aligned with the designated census tract. This process resulted the building polygons for the targeted community, as illustrated in Figure 3. Prior research (Abdulkarim et al. 2014; Shi et al. 2023) has utilized the Google Maps Service to analyze building types for urban planning and gather building envelope information for urban energy efficiency studies, due to its ability to offer highly accurate data on building types, polygons, and geolocations. Leveraging the geolocations of the building polygons acquired in this study, the author utilized the Google Maps API (Google for Developers n.d.) to collect information on the building types within the target community. In the designated study area, we have identified a total of 2,153 residential buildings and 43 commercial buildings, with the residential structures outnumbering the commercial ones by approximately a factor of 50. This ratio of residential to commercial buildings will later be applied in conjunction with the load served by each bus within the IEEE 13 Bus Test Feeder model. This approach aims to determine the specific number of residential and commercial buildings to be included in the simulation for this study.

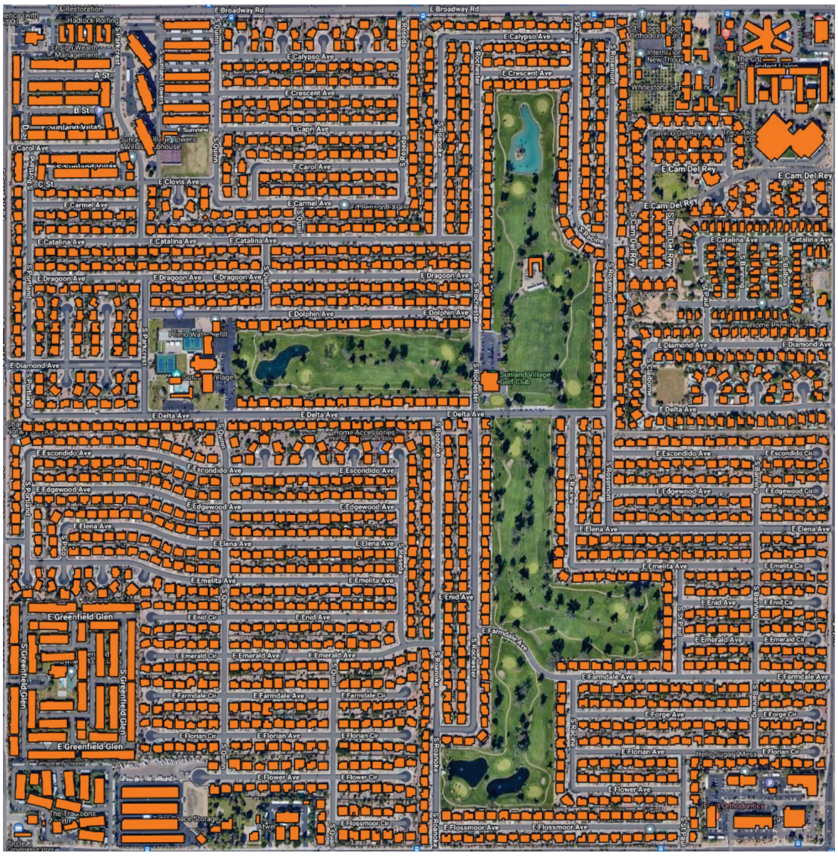

Figure 3. Building footprints in the target community.

(Microsoft Global Building Footprints Database)

DOE prototype buildings and weather files. This study adopted DOE prototype building models (DOE n.d.) for ASHRAE Climate Zone 2B (ASHRAE 2021), specially choosing Single Family House and Small Office models to represent residential and commercial buildings, respectively. Figure 4 illustrates the five internal thermal zones within the Small Office building model utilized in this study. Following the previous study (Pang et al. 2021), the Single Family House model is treated as having a single internal thermal zone. Typical Meteorological Year 3 (TMY3) weather files corresponding to this climate zone were utilized in the EnergyPlus simulations. Occupancy profiles generated earlier from human mobility modeling were integrated into these simulations to produce building power load data for each zone, along with the indoor environmental measurements such as zone temperature, wall temperature, internal heat gains. This information was subsequently applied to calibrate the

3R2C and 28R17C reduced-order thermal models, accurately reflecting the thermal dynamics of residential and commercial buildings, respectively. For control development purposes, we adopted RC model approach to represent the building energy dynamics within the proposed framework. Readers seeking further details on the building data are encouraged to consult the DOE official page (DOE n.d.) for the most up-to-date prototype building models.

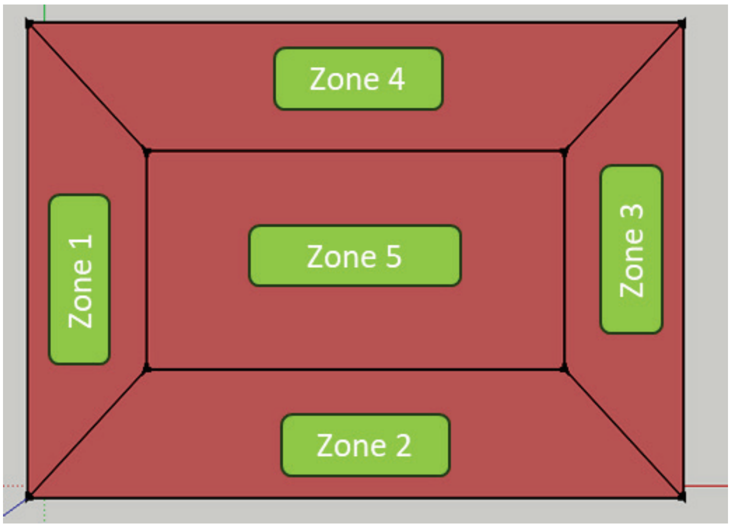

Figure 4. Internal thermal zones of the Small Office building DOE prototype model

Commercial Building occupancy profiles. Building occupancy profiles are essential for accurate energy and thermal modeling in buildings, informed by previous sections on human mobility patterns. For residential settings, such as Single Family Houses, a simple occupancy count is used, reflecting the inhabitants' mobility patterns. In contrast, commercial spaces, represented here by Small Office buildings, utilize the Lawrence Berkeley National Laboratory's Occupancy Simulator (Chen et al. 2018) to create detailed zone level and whole-building level occupancy profiles. These are then adjusted based on first arrival and last departure times from the occupants' mobility data. Following this tailored approach, Figure 5 shows the different occupancy profiles for two Small Office buildings used in this study.

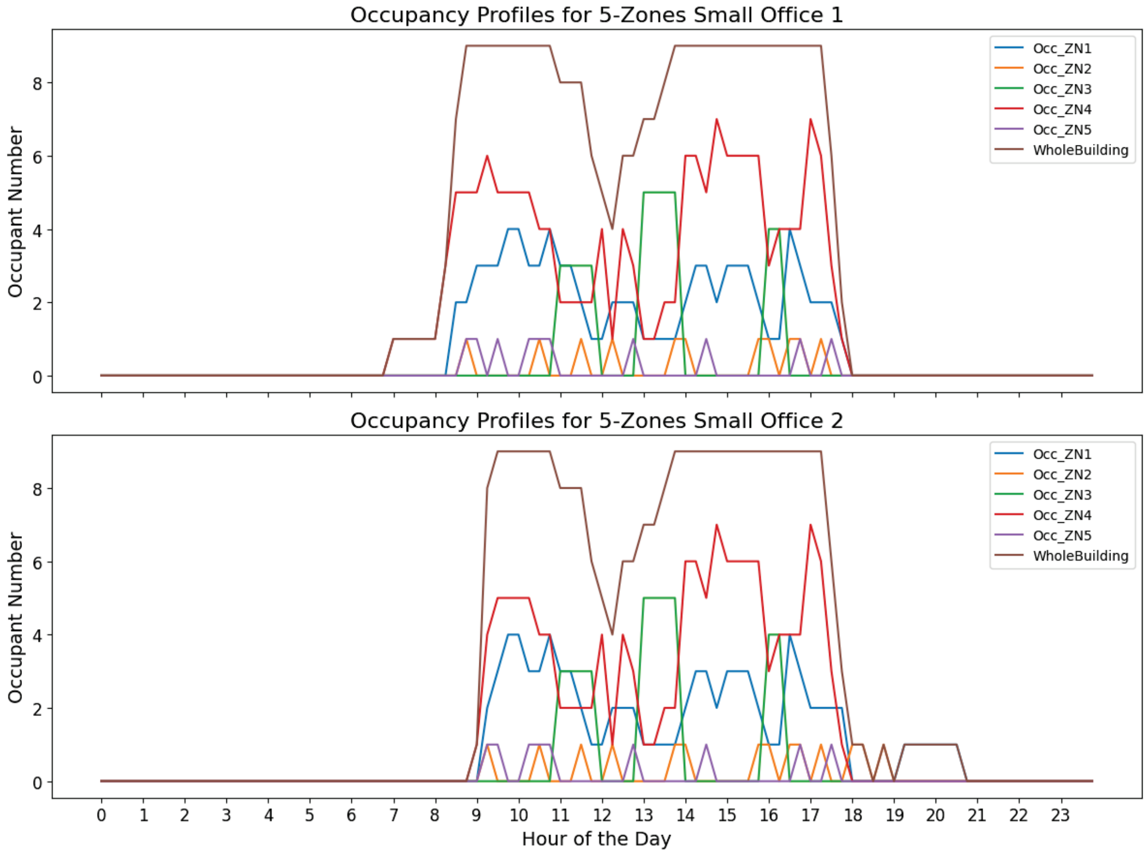

Figure 5. Dynamic occupancy profiles for Small Office

Building internal heat gains. Internal heat gains within buildings significantly influence energy consumption and thermal comfort. By utilizing the newly developed occupancy profiles for Small Office buildings, we've updated the zone-level internal heat gains, moving beyond the standard EnergyPlus schedules to better reflect the actual occupancy changes. This refinement ensures that the heat gains accurately represent the varying levels of activity throughout the building, directly impacting HVAC load requirements and energy efficiency. Figure 6 illustrates the updated internal heat gain profiles for two commercial buildings, showcasing the adjustments made to account for real-world occupancy patterns. These enhanced profiles have been integrated into the RC model calibration process, enabling a more precise simulation of thermal dynamics and energy consumption within these spaces.

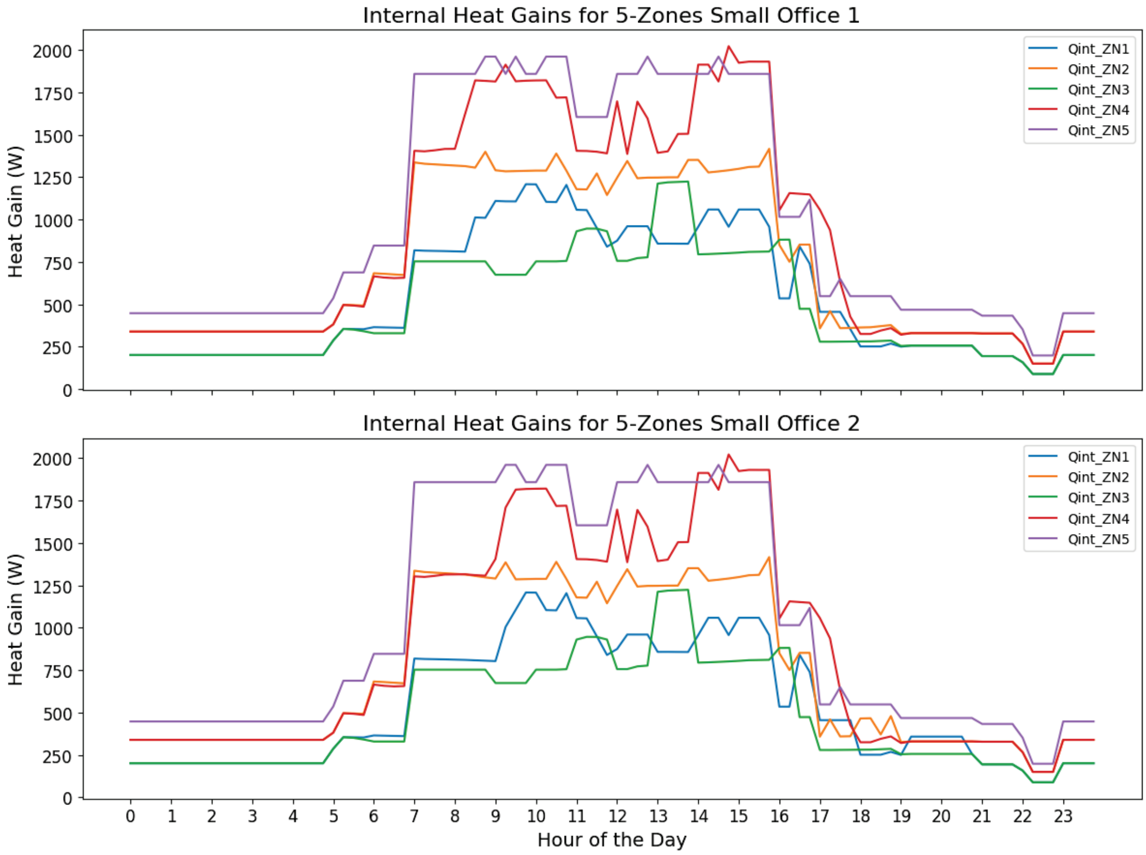

Figure 6. Internal heat gains for Small Office

Temperature setpoints. We have adopted the temperature setpoints and setbacks in accordance with ASHRAE Guideline 36 (ASHRAE 2018) recommendations. Recent studies (Zhang et al. 2020, 2022; Faulkner et al. 2023) have emphasized the significant benefits of adopting the ASHRAE Guideline 36 for HVAC system control, highlighting its potential to enhance energy efficiency, improve indoor air quality, and ensure control stability across various building environments. According to ASHRAE Guideline 36 (ASHRAE 2018), the daytime cooling setpoint for a single family house is set at 26°C when unoccupied, shifting to 24°C during occupied nighttime hours. For the Small Office, an occupied daytime cooling setpoint of 24°C is specified, with a temperature setback to 25°C when unoccupied, and a nighttime cooling setpoint of 29.5°C. Figure 7 illustrates the cooling setpoints and setbacks for individual zones and the entirety of the Small Office, indicating the operational schedule integrated into the RC model calibration process. This structured approach ensures the temperature control strategy is optimized for both comfort and energy conservation.

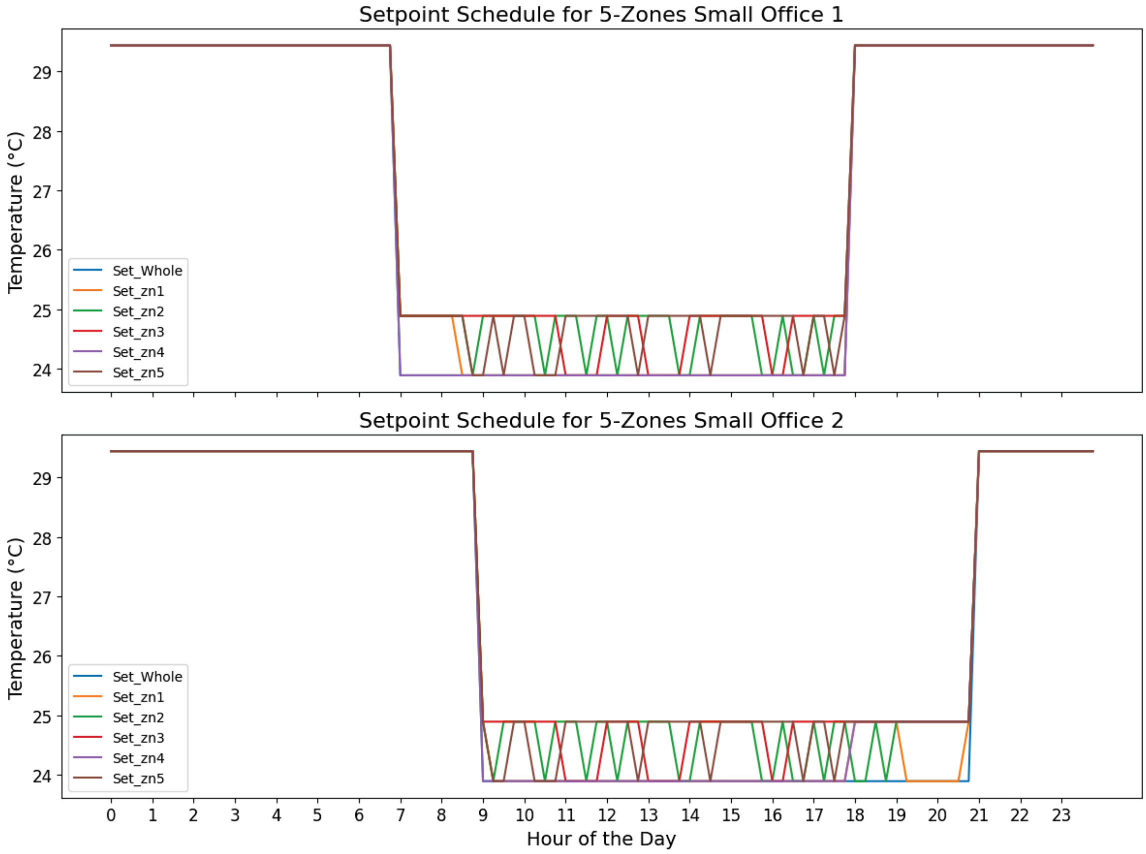

Figure 7. Temperature setpoints for Small Office

After collecting the aforementioned data, the model calibration was carried out in MATLAB. This process is framed as a nonlinear optimization problem, aiming to adjust the resistance (R) and capacitance (C) values within specified bounds. The goal is to minimize the discrepancy between the model's predicted zone temperatures and the actual observations obtained from EnergyPlus simulations. This approach seeks to enhance the accuracy of the thermal models across different zones within a building. For the calibration, data spanning from July 1 to July 31 was selected as the testing dataset, representing the summer season in Arizona, while data from August 11 to August 31 served as the training dataset. All data was generated through EnergyPlus simulations. The general steps in the RC model calibration process are as follows:

Define parameters and their bounds. In aligning with the RC model's architecture (3R2C and 28R17C), the calibration undertakes the optimization of a parameter set denoted as$r = \{r_1, r_2, r_3, \dots, r_i\}$, where i is represents the total count of parameters under optimization. This ensemble encompasses thermal resistance and capacitance values associated with the building's walls and zones, along with wall absorptance and window transmittance values related to solar radiation. It also includes the coefficient of performance (COP) for the HVAC system and the coefficient for internal heat gains. Drawing from the thermal property specifications within the EnergyPlus model and expert knowledge in the domain, boundaries for each parameter are established, denoted as lower bounds LB and upper bounds UB , thus: $LB = \{lb_1, lb_2, lb_3, \dots, lb_i\}, UB = \{ub_1, ub_2, ub_3, \dots, ub_i\}$. These bounds guarantee that the optimization algorithm explores solutions within a feasible and realistic space.

Objective function. The objective function is designed to minimize the sum of squared differences between the model predictions and actual observations across all temperature measurements for each zone. This objective function can be formulated as follows:

$$J(r) = \sum_{i=1}^{N} \sum_{j=1}^{K} \left(f(r)_{ij} - y_{true,ij}\right)^2 \qquad C.1$$

where N is the total number of data points, and K is the total number of zones. $y_{true,ij}$ represent the measurement data from EnergyPlus, and $f(r)_{ij}$ represents the model output based on the given set of parameters represented by r.

Optimization problem. In this process, the optimization problem can be defined as:

$$\min_{r} J(r) \quad C.2$$

Subjected to:

$$lb_i \leq r_i \leq ub_i, \forall i = 1, \ldots, M \quad C.3$$

where M is the total number of parameters to be optimized.

Evaluation metrics. After obtaining the optimal parameters r^*, the model performance will be evaluated using Mean Absolute Percentage Error (MAPE) for calibration and validation. This evaluation metric has been utilized by previous studies (Escrivá-Escrivá et al. 2011; Ma et al. 2017; Tardioli et al. 2020; Chong et al. 2021) to benchmark the performance of building energy models. In this study, the MAPE has been defined as:

$$MAPE = \frac{1}{N}\sum_{i=1}^{N}\left|\frac{f(r^*)_i - y_{true,i}}{y_{true,i}}\right| \quad C.4$$

where $f(r^*)_i$ is the model output based on the optimal parameters, and $y_{true,i}$ is the ground truth data from EnergyPlus. N is the total number of data points.

Building RC Model Calibration Results

Single-Zone residential building. Figure 8 presents the calibration results for a single-family house represented through a 3R2C model within the RC modeling framework, focusing exclusively on weekday data for calibration. The training dataset spans from July 1 to July 31, while the testing dataset covers August 11 to August 31, effectively simulating the cooling demands of the summer season. As highlighted in previous research (Bourdeau et al. 2019), the Mean Absolute Percentage Error (MAPE) is a widely adopted metric for assessing model performance in the context of building energy use modeling and forecasting. In this study, the training phase of the model yielded a MAPE of 3.2%, while the testing phase reported a slightly lower MAPE of 3.0%. As indicated by previous research (Jiang et al. 2023), the variance in temperature observed in the results can be attributed to the inherent delay in the calibrated RC model's response, contrasting with the instantaneous reaction of the idealized HVAC system simulated in EnergyPlus. Despite this limitation, the calibrated model successfully captures the overall trend of temperature fluctuations corresponding to the specified cooling load, illustrating its capability to replicate the thermal behavior of residential buildings accurately.

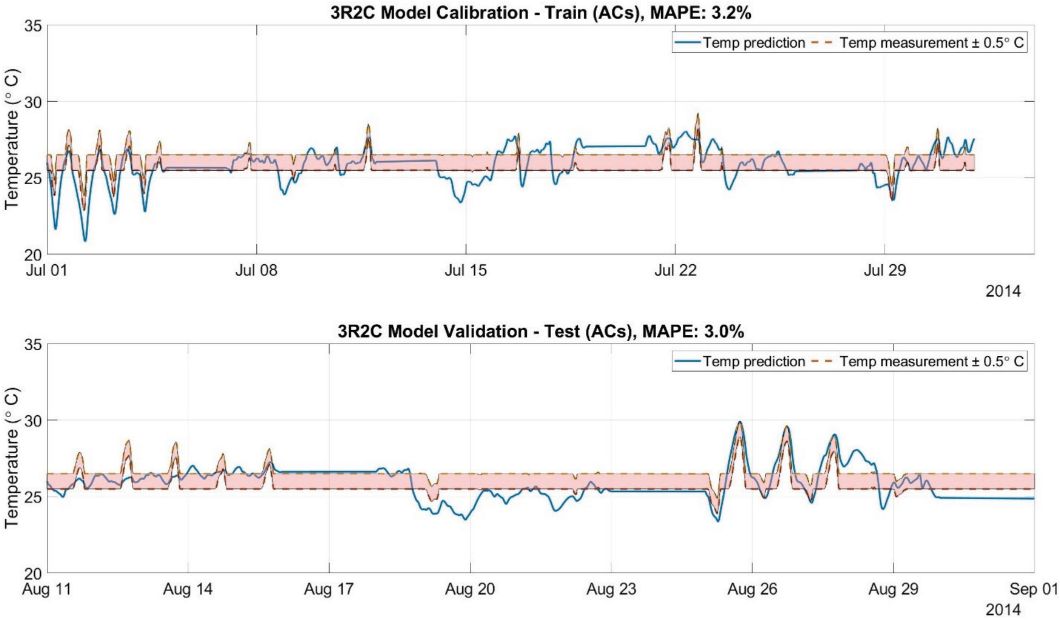

Figure 8. Single-zone residential building RC model calibration results

Utilizing the calibrated building RC model, we applied both MPC and a traditional rule-based ON/OFF control to assess the efficacy of MPC and to observe the model's response dynamics. As illustrated in Figure 9, within the predefined upper and lower temperature setpoint bounds, the ON/OFF control bounces back and forth, activating the HVAC system when the zone temperature surpasses the upper bound and deactivating it upon reaching the lower bound, demonstrating the typical behavior of ON/OFF control systems. In contrast, the temperature profile under MPC follows more closely to the upper temperature setpoint boundary. By solving an optimization problem that respects the temperature setpoint constraints and HVAC power limitations, MPC calculates the optimal HVAC operation for the current step with foresight into future conditions within the prediction horizon. Notably, the results highlight MPC's capacity for pre-cooling strategies in the afternoon before the occupants' return, adjusting to changes in temperature setpoints. Upon evaluating the total HVAC energy consumption over a single day of simulation, MPC achieved a 22.43% reduction in energy usage compared to the ON/OFF control approach, underscoring the superior energy efficiency of Model Predictive Control.

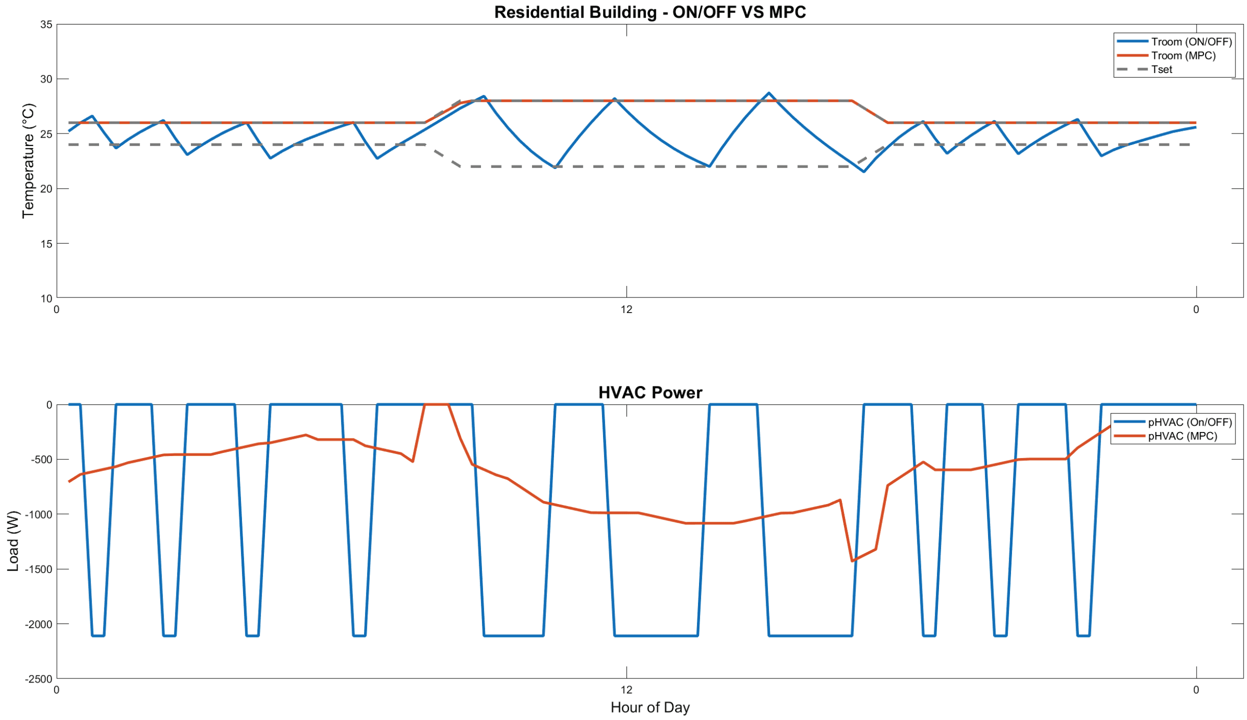

Figure 9. Single-zone residential building RC model MPC vs. ON/OFF control

Multi-Zone commercial building. For the Multi-Zone Commercial Building, the calibration of the five-zone small office's RC model was conducted in two stages: initial individual zone calibration followed by a comprehensive calibration integrating all five zones. The training period extended from July 1 to July 31, and the testing period from August 11 to August 31, mirroring the cooling requirements typical of the summer season. Calibration exclusively utilized weekday data to ensure accuracy reflective of regular operation. In this setup, each zone's HVAC system is controlled independently. Following figures, from Figure 11 to Figure 15, detail the calibration results for each zone, including measured and predicted temperature profiles, as well as MAPE for model training and testing. Figure 10 reveals that the training phase MAPE for each zone remains below 5%. These results indicate the model's proficiency in accurately capturing the temperature dynamics during both day and night.

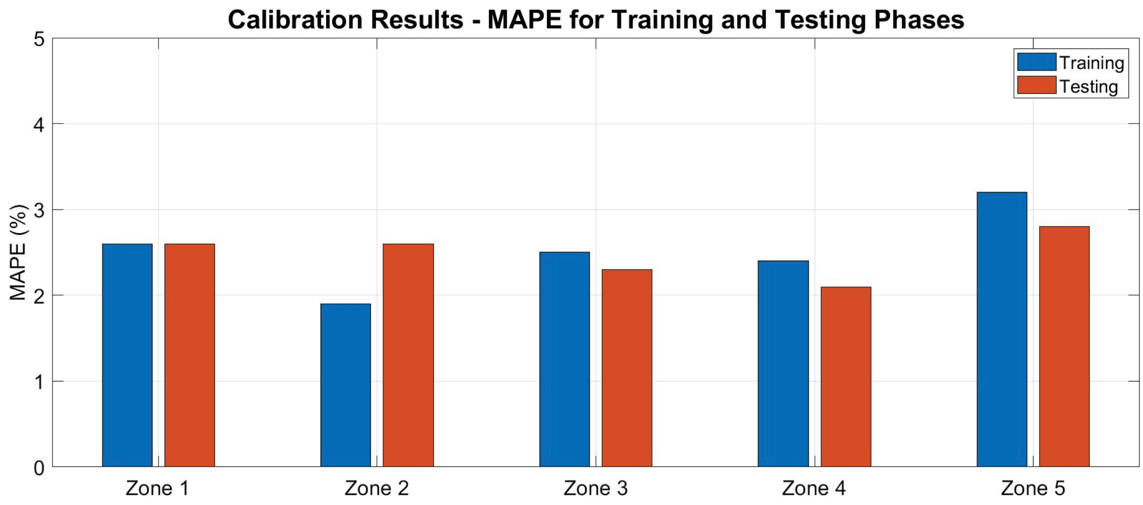

Figure 10. Summarized model calibration results by zone

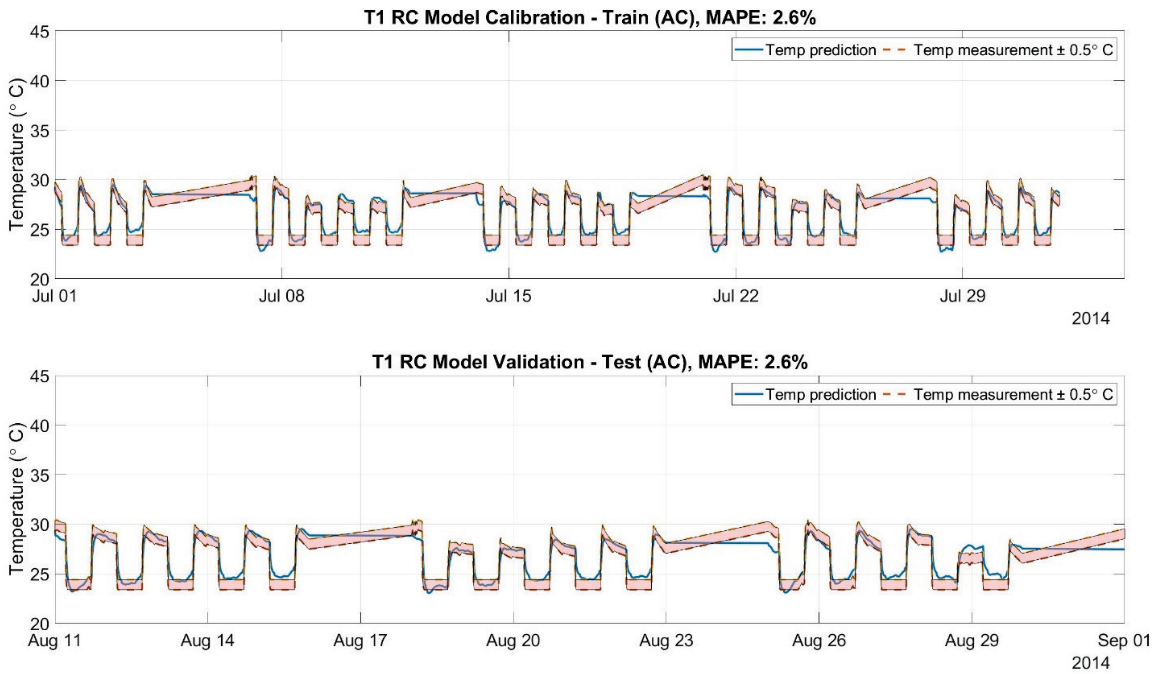

Figure 11. Five-zone commercial building RC model calibration results (Zone 1)

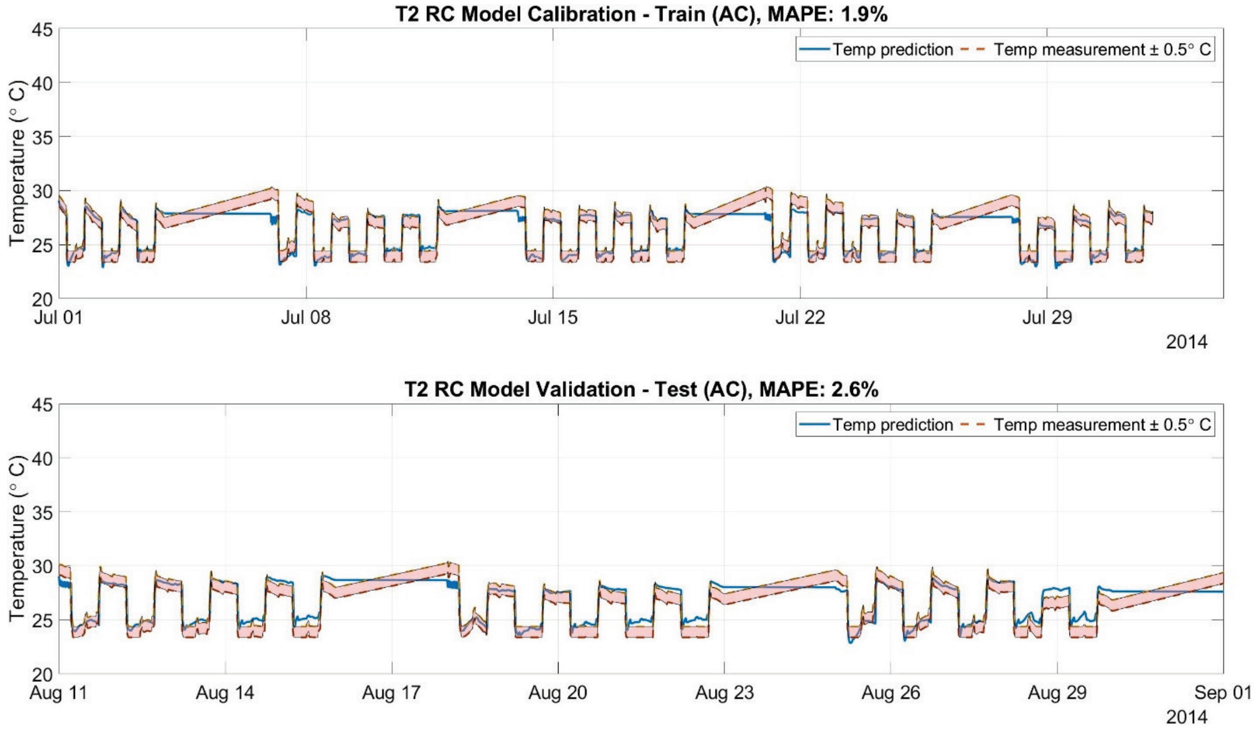

Figure 12. Five-zone commercial building RC model calibration results (Zone 2)

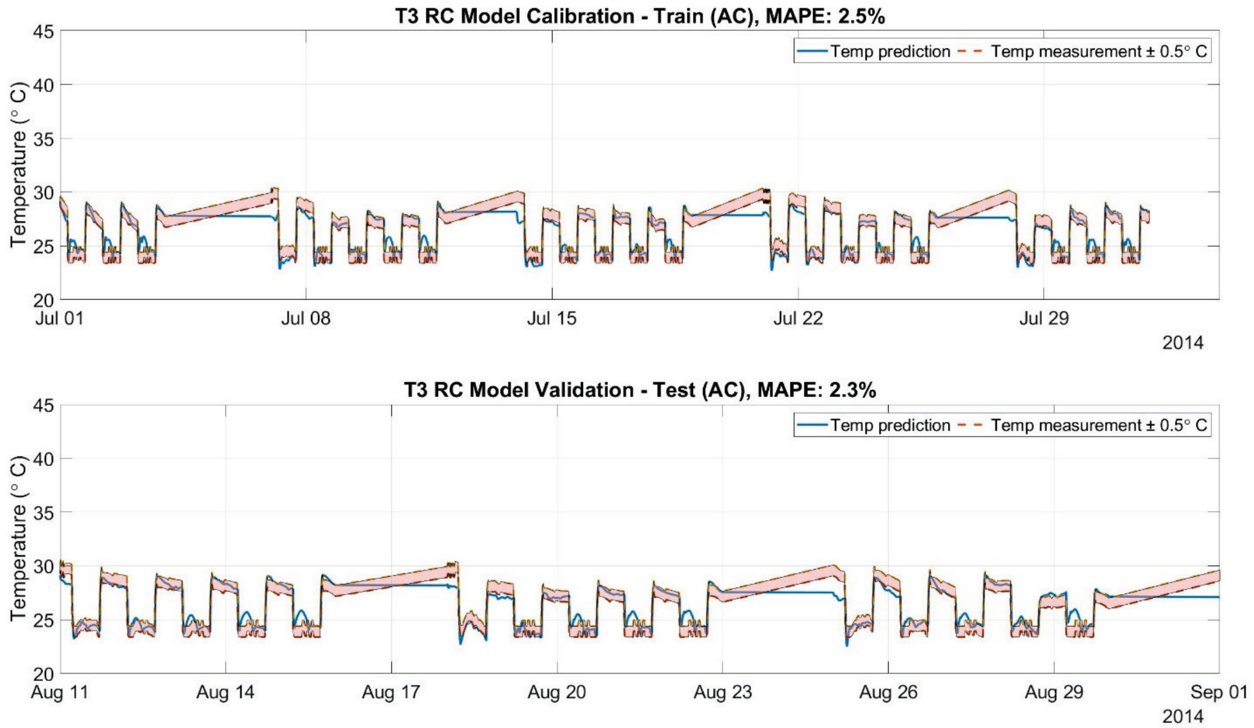

Figure 13. Five-zone commercial building RC model calibration results (Zone 3)

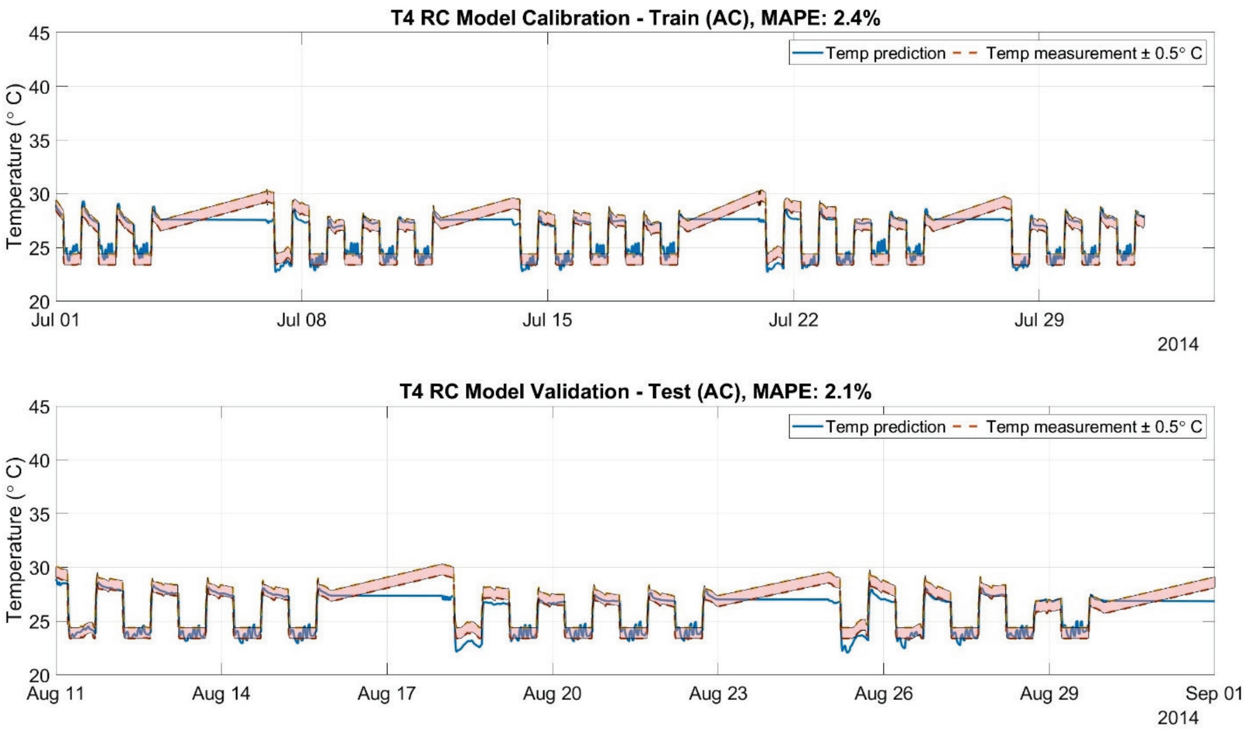

Figure 14. Five-zone commercial building RC model calibration results (Zone 4)

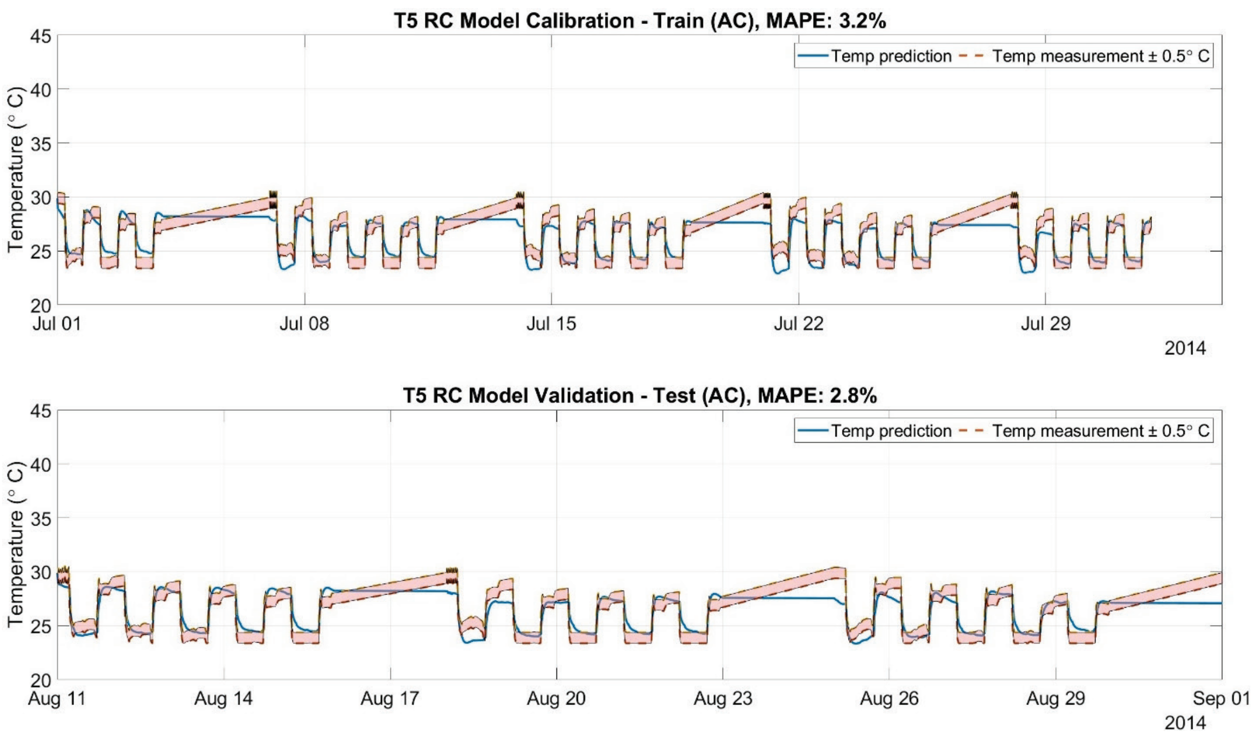

Figure 15. Five-zone commercial building RC model calibration results (Zone 5)

Built on the calibrated five-zone RC model, both MPC and traditional rule-based ON/OFF control was assessed to measure the MPC's effectiveness and to examine the model's thermal dynamics response. Figure 16 illustrates the performance under rule-based control across each zone, where a characteristic oscillation in zone temperature and corresponding HVAC load can be observed, mirroring results presented by the residential RC model. This commercial building RC model incorporates temperature setbacks in line with ASHRAE Guideline 36 (ASHRAE 2018), resulting in varying temperature setpoints across zones based on distinct occupancy patterns.

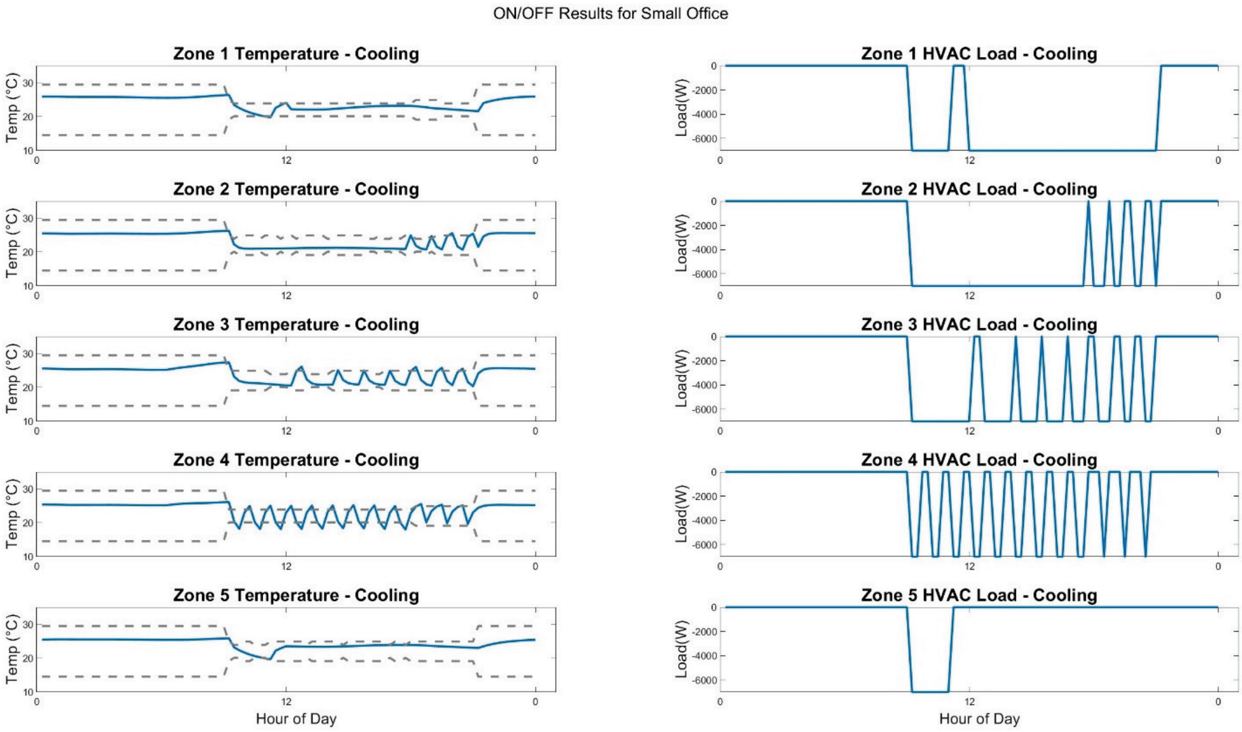

Figure 16. Five-zone commercial building RC model ON/OFF control results

Figure 17 displays MPC results, notably showcasing pre-cooling activity in the morning as the system transitions to daytime setpoints. By addressing an optimization challenge that adheres to temperature setpoint boundaries and HVAC power constraints, MPC formulates the ideal HVAC strategy for immediate steps while considering future conditions within the prediction horizon. An analysis of total HVAC energy consumption over a day's simulation revealed that MPC achieved a 22.85% energy savings in comparison to the ON/OFF control method, highlighting Model Predictive Control's enhanced efficiency.

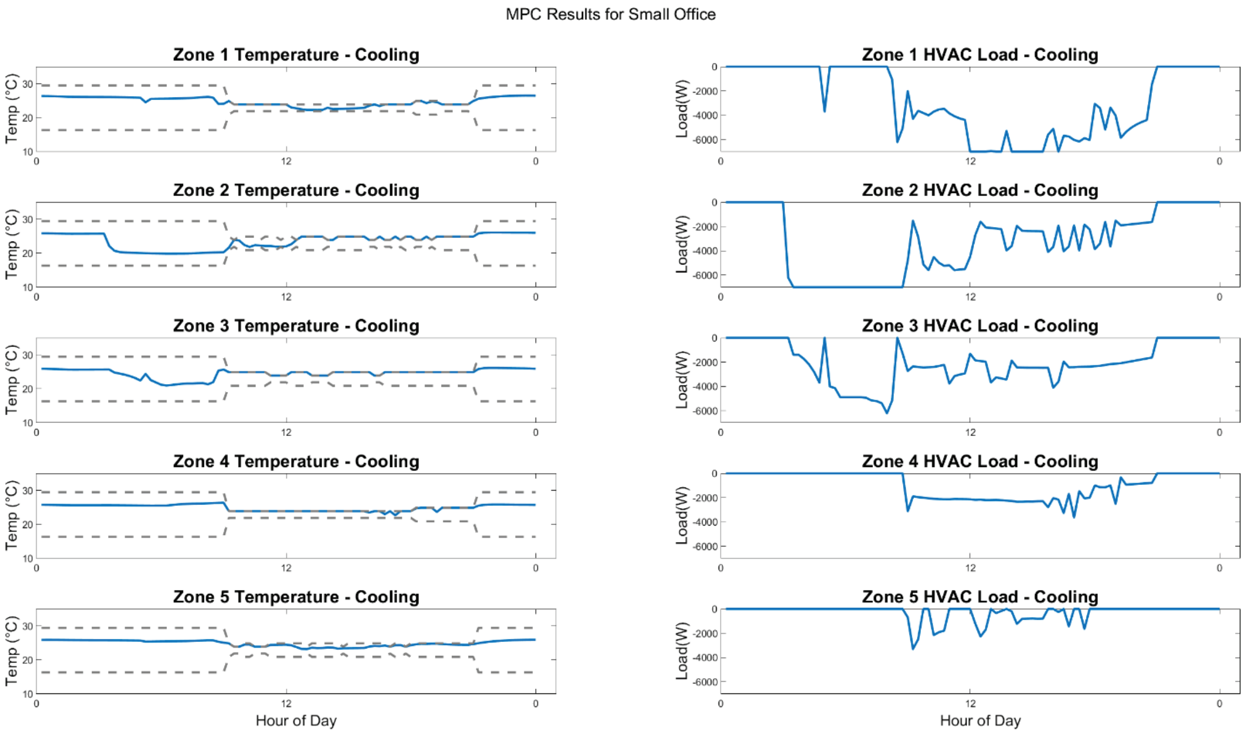

Figure 17. Five-zone commercial building RC model MPC results

References

Abdulkarim B, Kamberov R, Hay G (2014). Supporting urban energy efficiency with volunteered roof information and the google maps API. *Remote Sensing*, 6: 9691–9711.

ASHRAE (2018). ASHRAE Guideling 36: High Performance Sequences of Operation for HVAC Systems. ASHRAE.

ASHRAE (2021). ANSI/ASHRAE Addendum a to ANSI/ASHRAE Standard 169-2020. ASHRAE.

Bourdeau M, Zhai X, Nefzaoui E, et al. (2019). Modeling and forecasting building energy consumption: A review of data-driven techniques. *Sustainable Cities and Society*, 48: 101533.

Chen Y, Hong T, Luo X (2018). An agent-based stochastic occupancy simulator. *Building Simulation*, 11: 37–49.

Chong A, Gu Y, Jia H (2021). Calibrating building energy simulation models: A review of the basics to guide future work. *Energy and Buildings*, 253: 111533.

DOE (n.d.). Prototype Building Models. Building Energy Codes Program. Available at https://www.energycodes.gov/prototype-building-models. Accessed 7 Mar 2024.

Escrivá-Escrivá G, Álvarez-Bel C, Roldán-Blay C, et al. (2011). New artificial neural network prediction method for electrical consumption forecasting based on building end-uses. *Energy and Buildings*, 43: 3112–3119.

Faulkner CA, Lutes R, Huang S, et al. (2023). Simulation-based assessment of ASHRAE Guideline 36, considering energy performance, indoor air quality, and control stability. *Building and Environment*, 240: 110371.

Fontenot H, Ayyagari KS, Dong B, et al. (2021). Buildings-to-distribution-network integration for coordinated voltage regulation and building energy management *via* distributed resource flexibility. *Sustainable Cities and Society*, 69: 102832.

Google for Developers (n.d.). Google Maps Platform. Available at https://developers.google.com/maps. Accessed 6 Mar 2024.

Jiang Z, Qiu Y, Dong B (2023). Occupancy-based model predictive control for residential building cluster with photovoltaic and battery systems. In: Proceedings of International IBSPA Building Simulation Conference, Shanghai, China.

Liu Y (2024). Urban scale vehicle-to-building-to-grid integration leveraging human mobility modeling. PhD Thesis, Syracuse University, USA.

Liu Y, Dong B (2024). Modeling urban scale human mobility through big data analysis and machine learning. *Building Simulation*, 17: 3–21.

Ma W, Fang S, Liu G, et al. (2017). Modeling of district load forecasting for distributed energy system. *Applied Energy*, 204: 181–205.

Microsoft/GlobalMLBuildingFootprints (2024). Python. Microsoft. Available at https://github.com/microsoft/GlobalMLBuildingFootprints. Accessed 6 Mar 2024.

Pang Z, Chen Y, Zhang J, et al. (2021). How much HVAC energy could be saved from the occupant-centric smart home thermostat: A nationwide simulation study. *Applied Energy*, 283: 116251.

Shi Z, Silvennoinen H, Chadzynski A, et al. (2023). Defining archetypes of mixed-use developments using Google Maps API data. *Environment and Planning B*: *Urban Analytics and City Science*, 50: 1607–1623.

Tardioli G, Narayan A, Kerrigan R, et al. (2020). A methodology for calibration of building energy models at district scale using clustering and surrogate techniques. *Energy and Buildings*, 226: 110309.

Wu W, Dong B, Wang QR, et al. (2020). A novel mobility-based approach to derive urban-scale building occupant profiles and analyze impacts on building energy consumption. *Applied Energy*, 278: 115656.

Zhang K, Blum DH, Grahovac M, et al. (2020). Development and verification of control sequences for single-zone variable air volume system based on ASHRAEGuideline 36. In: Proceedings of the American Modelica Conference.

Zhang K, Blum D, Cheng H, et al. (2022). Estimating ASHRAE Guideline 36 energy savings for multi-zone variable air volume systems using Spawn of EnergyPlus. *Journal of Building Performance Simulation*, 15: 215–236.